REPORT

SEPARATIONS

Control of zeolite pore interior for chemoselective alkyne/olefin separations

Yuchao Chai[1]*, Xue Han[2]*, Weiyao Li[2], Shanshan Liu[1], Sikai Yao[1], Chong Wang[3], Wei Shi[4], Ivan da-Silva[5], Pascal Manuel[5], Yongqiang Cheng[6], Luke D. Daemen[6], Anibal J. Ramirez-Cuesta[6], Chiu C. Tang[7], Ling Jiang[3], Sihai Yang[2]†, Naijia Guan[1,4], Landong Li[1,4]†

The efficient removal of alkyne impurities for the production of polymer-grade lower olefins remains an important and challenging goal for many industries. We report a strategy to control the pore interior of faujasite (FAU) zeolites by the confinement of isolated open nickel(II) sites in their six-membered rings. Under ambient conditions, Ni@FAU showed remarkable adsorption of alkynes and efficient separations of acetylene/ethylene, propyne/propylene, and butyne/1,3-butadiene mixtures, with unprecedented dynamic separation selectivities of 100, 92, and 83, respectively. In situ neutron diffraction and inelastic neutron scattering revealed that confined nickel(II) sites enabled chemoselective and reversible binding to acetylene through the formation of metastable [Ni(II)(C_2H_2)$_3$] complexes. Control of the chemistry of pore interiors of easily scalable zeolites has unlocked their potential in challenging industrial separations.

More than 350 million metric tons of lower olefins (ethylene, propylene, and 1,3-butadiene) are produced each year through the steam cracking of hydrocarbons. Separating large quantities of chemical mixtures into purer forms accounts for an enormous amount of global energy consumption (*1*). To obtain polymer-grade olefins, the by-products of alkynes (acetylene, propyne, and butyne) in the stream must be reduced to <5 parts per million (ppm), because these alkynes irreversibly poison the catalysts for polymerization (*2*). State-of-the-art techniques to purify olefins are based on the partial hydrogenation of alkynes over supported Pd-catalysts; however, such methods suffer from poor selectivity and high costs (*3*). Emerging porous sorbents, notably metal-organic frameworks (MOFs), show preferential adsorption of alkynes over olefins, suggesting alternative adsorption-based purification processes for ethylene (*4*–*8*) and propylene (*9*–*11*).

However, such processes have yet to be commercialized because of the inherently limited stability and high production costs of MOFs. Additionally, the primary physisorption mechanism in MOFs that drives separations results in a trade-off between adsorption selectivity and capacity.

Zeolites have structural robustness and low-cost production, and they are widely used for industrial separations on the basis of their molecular sieving property (*12*), but they are not effective for alkyne/olefin separations because these molecules have similar molecular sizes and volatilities (*13*). Zeolites can act as useful scaffolds to stabilize active metal sites to uncover previously unidentified functions and properties. In this work, we confine isolated Ni(II) sites into faujasite (FAU) zeolite to achieve remarkable adsorption of alkynes from a range of alkyne/olefin mixtures. The strong yet fully reversible binding between alkyne and the open Ni(II) sites results in the formation of metastable [Ni(alkyne)$_3$] complexes under dynamic conditions and enables the complete removal of alkynes from olefins (alkynes <1 ppm). The facile production and high stability of Ni@FAU reinforce its potential in the industrial purification of lower olefins.

M@FAU zeolites [M = Ni(II), Cu(II), and Zn(II)] were synthesized from hydrothermal reactions of mixed gels {molar ratio of SiO_2:Al_2O_3:Na_2O:M-TAPTS:H_2O = 7.8:1.0:2.2:0.6:174; TAPTS = 3-[2-(2-aminoethylamino)ethylamino]propyltrimethoxysilane} and subsequent processing (yield, 77 to 85%). The TAPTS ligand was used to coordinate Ni(II) ions for their inclusion in the zeolite pore structure at locations that can be difficult to access during conventional post-synthesis ion-exchange. Similar approaches based on (3-mercaptopropyl)trimethoxysilane ligand have been reported to introduce metal sites or clusters into desirable sites of various zeolites, showing excellent catalytic activities (*14*, *15*). Synchrotron x-ray powder diffraction data confirmed that M@FAU zeolites crystallize in the cubic space group, $Fd\bar{3}m$, adopting the FAU-topology, and there is an absence of bulk phase of metal oxides (fig. S1 and table S1).

The homogeneous distribution of transition-metal cations throughout the M@FAU crystals (3 to 5 μm) were confirmed by electron microscopy (figs. S2 and S3). Under ambient conditions, the pores of M@FAU samples were filled with water molecules that could be removed completely by heating to 623 K (fig. S4). The divalent oxidation state of the confined metal ions was confirmed by x-ray photoelectron spectroscopy (fig. S5), and the primary location of confined Ni(II) sites in FAU zeolite was studied using density functional theory (DFT) calculations (fig. S6) and in situ neutron powder diffraction (NPD) studies.

The adsorption capacities of desolvated M@FAU and the parent Na-FAU were first evaluated by measuring the adsorption isotherms of C_2H_2 and C_2H_4 (Fig. 1A and figs. S7 and S8). At 1 bar and 298 K, Ni@FAU, [$Ni_{12}Na_{20}(Al_{44}Si_{148}O_{384})$], showed lower overall uptakes of C_2H_2 [3.48 mmol/g; equivalent to ~3.7 C_2H_2 per Ni(II) site] and C_2H_4 (2.36 mmol/g) compared with that of Na-FAU (5.15 and 4.06 mmol/g, respectively), because of the moderate decrease of Brunauer-Emmett-Teller surface areas on incorporation of Ni(II) sites (from 710 to 531 m^2/g; fig. S9). Notably, 2.0 mmol/g of C_2H_2 uptake was recorded in Ni@FAU at 0.02 bar, a pressure that is relevant to the partial pressure of C_2H_2 impurity in industrial C_2H_4 streams. The steep C_2H_2 uptake of Ni@FAU at low pressure was consistent with its higher heat of adsorption (48.6 kJ/mol) than that of Na-FAU (21.7 kJ/mol) and of C_2H_4 uptake in Ni@FAU (25.8 kJ/mol), which were determined by differential scanning calorimetry (figs. S10 to S21, table S2, and supplementary text).

Temperature-programmed desorption (TPD) profiles of C_2H_2- and C_2H_4-loaded Ni@FAU revealed higher adsorption uptake of C_2H_2 (1.75 mmol/g) than of C_2H_4 (0.51 mmol/g) and showed desorption peaks centered at 363 and 329 K, respectively. When coadsorbed with an equimolar mixture of C_2H_2/C_2H_4, the TPD profile resembled that of C_2H_2-loaded Ni@FAU, and little desorption of C_2H_4 was observed. Moreover, the pre-adsorbed C_2H_4 molecules in Ni@FAU could be readily displaced by C_2H_2 under dynamic conditions (Fig. 1B). The presence of strongly bound C_2H_2 molecules in Ni@FAU is also confirmed by in situ Fourier transform infrared (FTIR) studies at 298 K (Fig. 1C). On adsorption in Ni@FAU, ν_{as}(CH) and ν_s(CH) bands of C_2H_2 red-shifted to 2925 and 3010 cm^{-1}, respectively, compared with gaseous or physisorbed C_2H_2 (3100 to 3400 cm^{-1}) (*16*, *17*), whereas no shift was observed for adsorbed C_2H_4 molecules.

[1]School of Materials Science and Engineering and National Institute for Advanced Materials, Nankai University, Tianjin 300350, China. [2]Department of Chemistry, The University of Manchester, Manchester, M13 9PL, UK. [3]State Key Laboratory of Molecular Reaction Dynamics, Dalian Institute of Chemical Physics, Chinese Academy of Sciences, Dalian 116023, China. [4]Key Laboratory of Advanced Energy Materials Chemistry of Ministry of Education, Nankai University, Tianjin 300071, China. [5]ISIS Facility, Science and Technology Facilities Council (STFC), Rutherford Appleton Laboratory, Chilton, Oxfordshire, OX11 0QX, UK. [6]Neutron Scattering Division, Neutron Sciences Directorate, Oak Ridge National Laboratory (ORNL), Oak Ridge, TN 37831, USA. [7]Diamond Light Source, Harwell Science and Innovation Campus, Didcot, Oxfordshire, OX11 0DE, UK.
*These authors contributed equally to this work.
†Corresponding author. Email: sihai.yang@manchester.ac.uk (S.Y.); lild@nankai.edu.cn (L.L.)

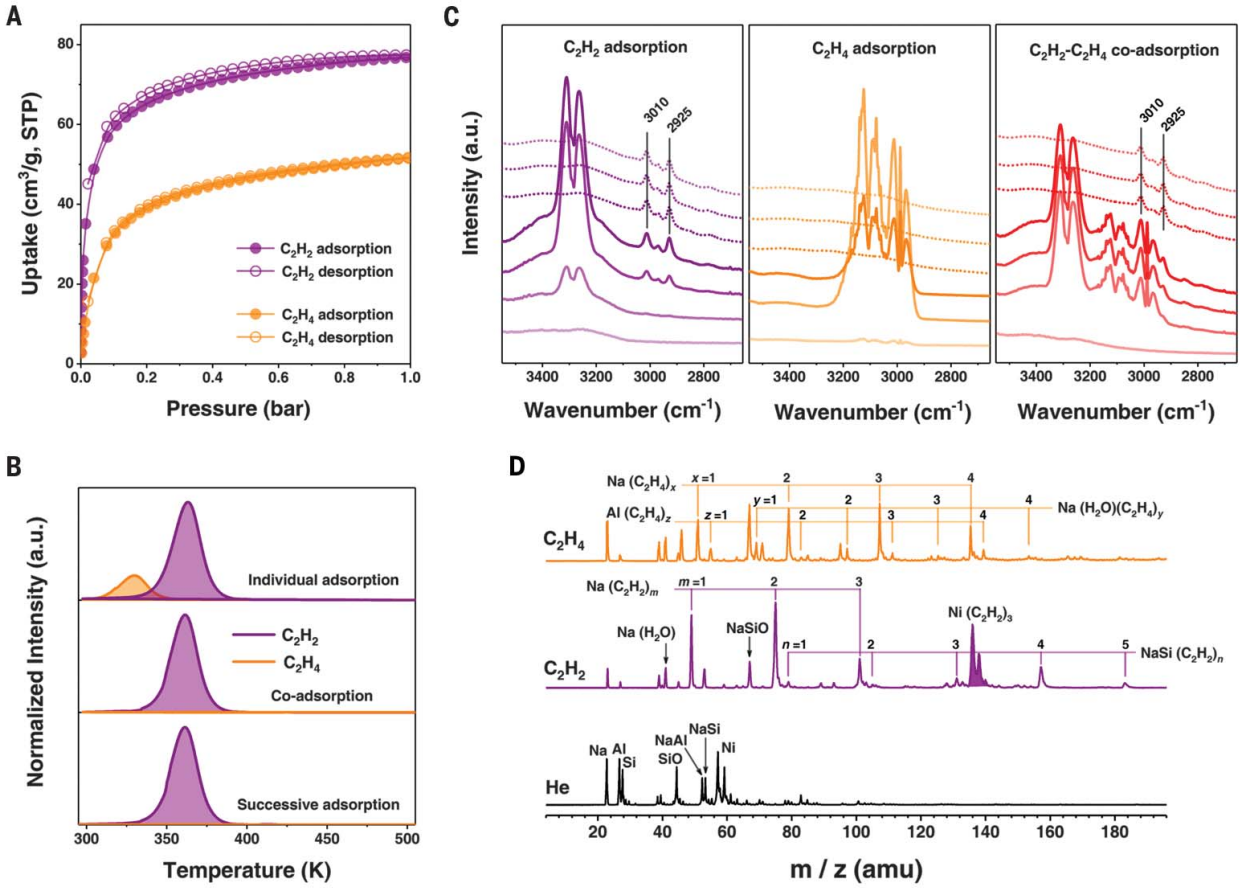

Fig. 1. Adsorption data of C_2H_2 and C_2H_4 for Ni@FAU. (**A**) Adsorption isotherms of C_2H_2 and C_2H_4 for Ni@FAU at 298 K. STP, standard temperature and pressure. (**B**) TPD profiles of C_2H_2- and C_2H_4-adsorbed Ni@FAU after their individual adsorption, coadsorption, and successive adsorption (first C_2H_4 and then switched to C_2H_2) at 298 K. a.u., arbitrary units. (**C**) In situ FTIR spectra of Ni@FAU on adsorption of C_2H_2 and C_2H_4 followed by He purging (dotted lines) at 298 K. (**D**) Mass spectra of species produced by pulsed laser vaporization of the Ni@FAU target in the presence of carrier gas He, C_2H_2 (2%)/He, and C_2H_4 (2%)/He. m/z, mass/charge ratio; amu, atomic mass unit.

Infrared bands of bound C_2H_2 molecules were observed in the equimolar C_2H_2/C_2H_4 coadsorbed Ni@FAU, demonstrating the selective uptake of C_2H_2 under competitive adsorption.

The adsorption species in C_2H_2- and C_2H_4-loaded Ni@FAU were identified by mass spectrometry (*18*). The pulsed laser vaporization of Ni@FAU target in He produced a series of fragments, and Ni-containing fragments can be distinguished by the characteristic isotope ratio of nickel (^{58}Ni:^{60}Ni = 68%:26%). On the basis of the control experiment of metallic Ni and Na-FAU (figs. S22 and S23), fragments corresponding to $Ni(C_2H_2)_3$ species were identified as a key species in C_2H_2-adsorbed Ni@FAU (Fig. 1D), whereas no $Ni(C_2H_4)_n$ (n = 1 to 4) species were observed for C_2H_4-adsorbed Ni@FAU. These results demonstrated the highly selective adsorption of C_2H_2 in Ni@FAU and its high capability to remove trace C_2H_2 from the C_2H_4 stream.

The ability of M@FAU (M = Ni, Cu, and Zn) to separate C_2H_2/C_2H_4 mixtures under dynamic conditions was evaluated by breakthrough experiments. All of the samples showed sufficient dynamic adsorption of C_2H_2 and could produce ultrapure C_2H_4 (C_2H_2 <1 ppm) streams at the outlet of the fixed beds at 298 K (Fig. 2A and figs. S24 and S25). The dynamic C_2H_2 uptakes calculated from column breakthrough curves (2% C_2H_2:2% C_2H_4) were 0.91, 1.26, and 1.72 mmol/g for Zn@FAU, Cu@FAU, and Ni@FAU, respectively. The dynamic C_2H_2 uptake of Ni@FAU remained the same when the C_2H_4 concentration was increased to 50% or the C_2H_2 concentration decreased to 1% (Fig. 2B). This capability is distinct to the porous sorbents functioning solely through physisorption (*6*), which show rapid reductions of dynamic uptakes with decreasing gas concentrations.

Furthermore, this dynamic uptake compared favorably to the leading MOFs—for example, 1.70 mmol/g of JCM-1 (*19*), 1.18 mmol/g of UTSA-200a (*20*), 1.23 mmol/g of NbU (*21*), and 0.73 mmol/g of SIFSIX-2-Cu-i (*4*). Additionally, Ni@FAU showed a higher overall acetylene productivity (116.8 mmol/g) compared with that of leading MOFs, such as NKMOF-1-Ni (96.0 mmol/g) (*8*), UTSA-200a (85.7 mmol/g) (*20*), and SIFSIX-2-Cu-i (53.3 mmol/g) (*4*). Also, Ni@FAU exhibited a very low dynamic uptake of C_2H_4 (0.02 mmol/g) under the same conditions, and a remarkable C_2H_2/C_2H_4 dynamic selectivity of ~100 was achieved, compared with reported state-of-the-art sorbents (table S3). A comparison of experimentally determined C_2H_2/C_2H_4 dynamic selectivity against the dynamic uptake of C_2H_2 demonstrated the remarkable performance of Ni@FAU for C_2H_2/C_2H_4 separation (Fig. 2C).

We observed similar separation capability with Ni@FAU after increasing the column temperature from 298 to 308 K (fig. S26) or adding CO_2 or H_2O into the gas stream (fig. S27), whereas an ~25% decrease in the adsorption capability of C_2H_2 was observed for a Ni@FAU sample that has been preadsorbed with H_2O (fig. S28). The performance of Ni@FAU was further evaluated at 5 bar, where excellent C_2H_2/C_2H_4 separations were observed and the dynamic uptakes of C_2H_2 and C_2H_4 increased to 2.25 and 0.39 mmol/g, respectively (fig. S29). Moreover, Ni@FAU could be used to separate mixtures of propyne/propylene, butyne/1,3-butadiene, and acetylene/propylene with high dynamic alkyne uptakes of 1.58 to 1.80 mmol/g

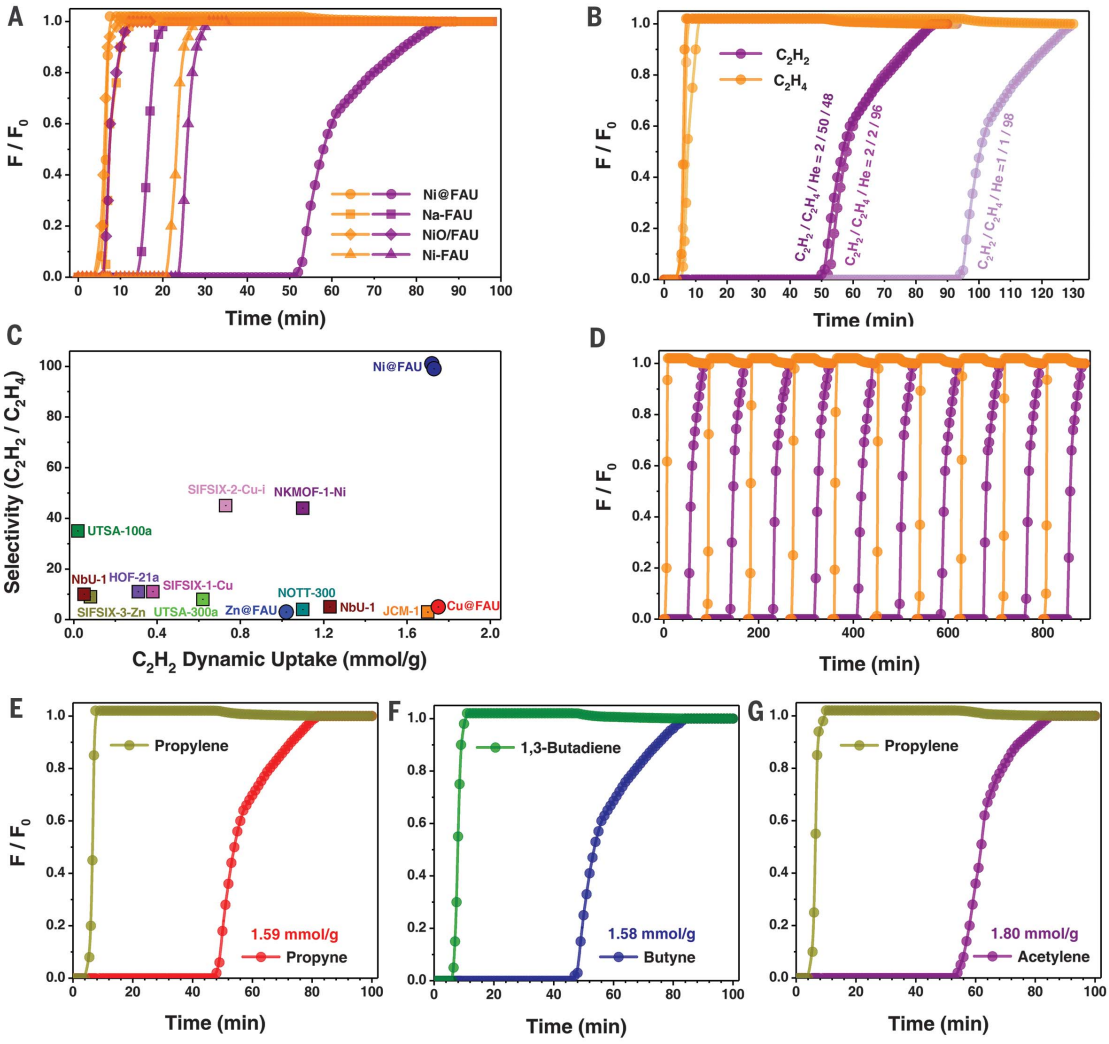

Fig. 2. Column breakthrough studies for alkyne/olefin separations. (**A**) Column breakthrough curves for a C_2H_2/C_2H_4 (2%/2%) mixture using various zeolite samples at 298 K. C_2H_2 and C_2H_4 are shown in purple and orange, respectively. F, flow rate; F_0, initial flow rate. (**B**) Effects of feed gas composition on C_2H_2/C_2H_4 separation over Ni@FAU at 298 K. (**C**) Plot of C_2H_2/C_2H_4 dynamic selectivity against C_2H_2 dynamic uptake under ambient conditions with state-of-the-art sorbent materials. (**D**) View of recyclability of Ni@FAU for the separation of C_2H_2/C_2H_4 (2%/2%) at 298 K. Sample regeneration was achieved by treatment in He at 423 K for 30 min. (**E** to **G**) Column breakthrough curves for propyne/propylene (2%/2%) (E), butyne/1,3-butadiene (2%/2%) (F), and acetylene/propylene (2%/2%) (G) over fixed beds packed with Ni@FAU at 298 K. Total gas flow, 6.0 mL/min; sample weight, 0.2 g.

and notable breakthrough selectivities of 92, 83, and 109, respectively, under ambient conditions (Fig. 2, E to G).

These results signal the potential of Ni@FAU for the adsorptive removal of alkynes from industrial olefin streams. Practical sorbents must be recyclable. After 10 cycles of C_2H_2/C_2H_4 separations with Ni@FAU, we observed no decline in the retention time and full sorbent regeneration at 373 K between each cycle (Fig. 2D). In contrast, Cu@FAU exhibited poor reversibility for C_2H_2/C_2H_4 separations because of the formation of oligomers on Cu(II) sites blocking the pores (fig. S30). To understand the role of Ni(II) in Ni@FAU, we introduced the metal ions into the FAU zeolites using different methods, such as ion-exchange (denoted as Ni-FAU) or wet impregnation (denoted as NiO/FAU) (figs. S31 and S32). These two samples exhibited very poor separation of C_2H_2/C_2H_4 (Fig. 2A), which suggests that the excellent performance of Ni@FAU originates from its binding environment of the confined Ni(II) sites within the pores.

In situ NPD studies enabled identification of the locations of the confined Ni(II) sites and the adsorbed gas (C_2D_2, C_2D_4, C_3D_4, and C_3D_6) molecules within Ni@FAU (figs. S33 to S38 and table S4). Fourier difference map analysis of the desolvated Ni@FAU [$Ni_{12}Na_{20}(Al_{44}Si_{148}O_{384})$] confirmed the structural integrity and the absence of residual nuclear density in the supercage. In-depth analysis revealed apparent residual nuclear density near the six-membered ring of the sodalite cage, which we assigned as Ni(II) ions stabilized by framework oxygen centers (fig. S39). This assignment is consistent with DFT calculations (fig. S6). By contrast, Ni(II) sites within Ni-FAU were primarily hexagonal prism sites, which were sterically hindered by the highly confined void (diameter of ~2.5 Å) for gas binding. This finding was consistent with its poor separation performance (fig. S40 and supplementary text).

Upon gas loading, variations in Bragg peak intensities were observed, and the binding domains of gases were successfully interpreted by Fourier difference map analysis (Fig. 3, A to E) and Rietveld refinements. At low loading in $[Ni_{12}Na_{20}(Al_{44}Si_{148}O_{384})]\cdot(C_2D_2)_{12}$ (equivalent to ~1 mmol/g C_2D_2 uptake), all adsorbed C_2D_2 molecules were located at a single site, which is distributed over six equivalent positions in the supercage and exhibited a side-on interaction to the Ni(II) sites [$C\cdots Ni = 3.87$ to 4.08 Å, $\angle C \equiv C \cdots Ni = 91.1°$], which suggests the binding interaction between the C≡C bond and Ni(II) centers (fig. S41). Additionally, supplementary hydrogen bonds between $D_{C_2D_2}$ and framework oxygen were observed [$D\cdots O = 2.99$ Å, $\angle C\text{–}D\cdots O = 161°$] (Fig. 3B). A similar host-guest binding mechanism [$C\cdots Ni = 3.83$ to 4.05 Å, $\angle C\equiv C\cdots Ni = 91.9°$] was observed in $[Ni_{12}Na_{20}(Al_{44}Si_{148}O_{384})]\cdot(C_2D_2)_{26}$ (equivalent to ~2.3 mmol/g C_2D_2 uptake) with weaker hydrogen bonds to the framework oxygen [$D\cdots O = 3.27$ Å, $\angle C\text{–}D\cdots O = 151°$]. The overall binding geometry is in marked agreement with cation-acetylene π complexation (*13*, *22*). X-ray absorption near-edge structure (XANES) analysis confirmed the retention of a divalent oxidation state of Ni(II) sites on

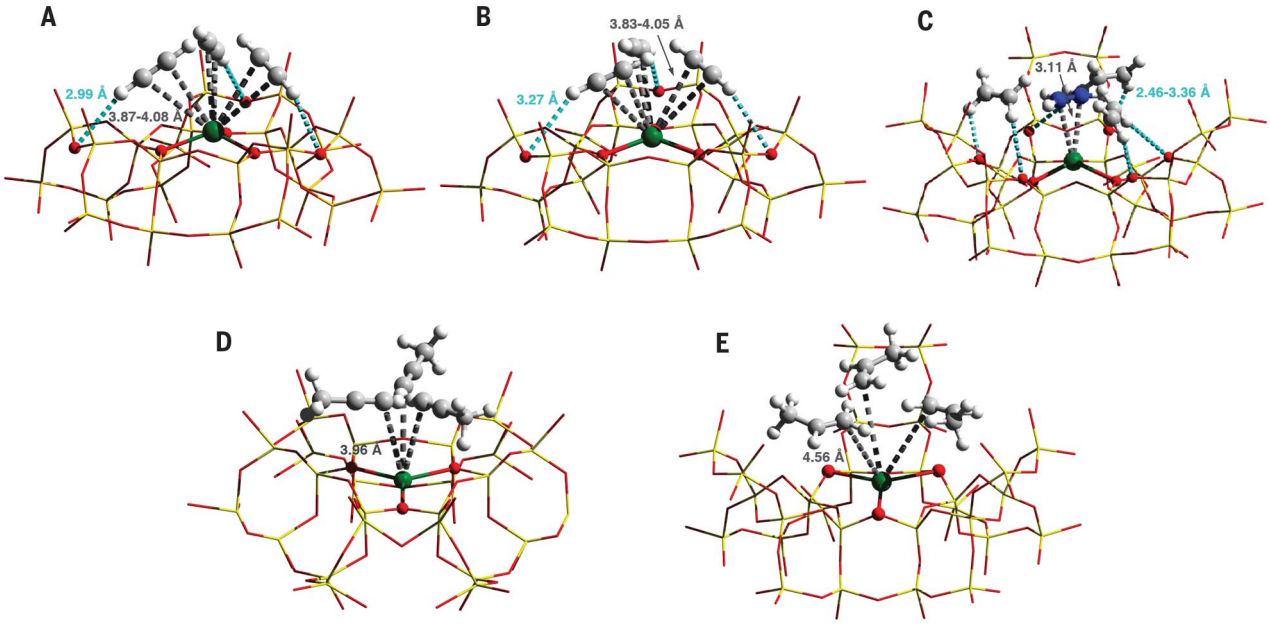

Fig. 3. Views of crystal structures for the Ni@FAU zeolite as a function of gas loading. All structures were derived from Rietveld refinements of NPD data at 7 K [Si and Al: yellow; O: red; Ni: green; C: gray; D: white; C_2D_4 (**1**) is highlighted in blue for clarity]. The host-guest interactions are highlighted by dashed lines, and the estimated standard deviation values for binding distances are typically within 0.02 to 0.08 Å. Views are of binding sites for adsorbed gas molecules in $[Ni_{12}Na_{20}(Al_{44}Si_{148}O_{384})]\cdot(C_2D_2)_{12}$ (**A**), $[Ni_{12}Na_{20}(Al_{44}Si_{148}O_{384})]\cdot(C_2D_2)_{26}$ (**B**), $[Ni_{12}Na_{20}(Al_{44}Si_{148}O_{384})]\cdot(C_2D_4)_{17}$ (**C**), $[Ni_{12}Na_{20}(Al_{44}Si_{148}O_{384})]\cdot(C_3D_4)_{20}$ (**D**), and $[Ni_{12}Na_{20}(Al_{44}Si_{148}O_{384})]\cdot(C_3D_6)_{26}$ (**E**).

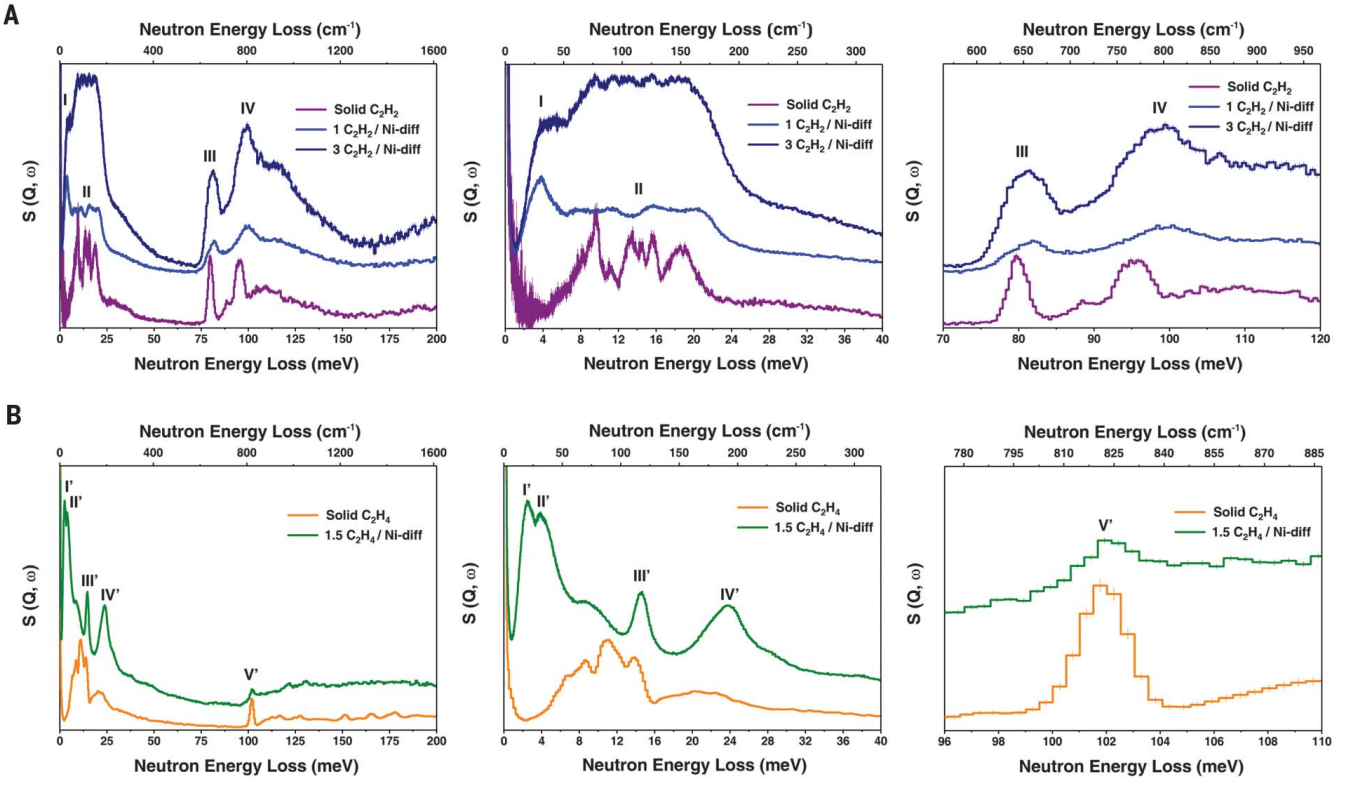

Fig. 4. INS spectra for Ni@FAU as a function of gas loading. (**A**) Comparison of INS spectra of C_2H_2-loaded Ni@FAU and that of solid C_2H_2. (**B**) Comparison of INS spectra of C_2H_4-loaded Ni@FAU and that of solid C_2H_4. Enlarged details show the translational or librational and the internal vibrational modes of adsorbed C_2H_2 and C_2H_4 molecules. Difference spectra were produced by removing signals of the bare zeolite and sample holder. Raw spectra are provided in the supplementary materials. Peaks are labeled with Roman numerals. S, dynamic structure factor; Q, momentum transfer; ω, frequency change.

acetylene binding (fig. S42), and no elongation of C–C distance in bound C_2D_2 was found in the NPD analysis. These results were consistent with the selective yet reversible sorption.

However, $[Ni_{12}Na_{20}(Al_{44}Si_{148}O_{384})]\cdot(C_2D_4)_{17}$ (equivalent to ~1.5 mmol/g C_2D_4 uptake) exhibited a different binding geometry with two distinct sites (**1** and **2**) in the supercage (fig. S41). C_2D_4 (**1**) molecules (accounting for ~40% of adsorbed C_2D_4) interact with Ni(II) $[C\cdots Ni = 3.11\,Å, \angle C=C\cdots Ni = 77.8°]$ in a similar side-on manner to that of C_2D_2, whereas C_2D_4 (**2**) (accounting for ~60% of adsorbed C_2D_4) showed no interaction with Ni(II) but did show multiple hydrogen bonds to the framework oxygen $[D\cdots O = 2.46$ to $3.36\,Å, \angle C-D\cdots O = 124$ to $178°]$. These NPD studies revealed the explicit difference between C_2D_2 and C_2D_4 upon adsorption in Ni@FAU. Additional π electrons in C_2D_2 and its linear geometry (and thus low spatial hindrance) enabled the formation of metastable $[Ni(II)(C_2D_2)_3]$ complexes in the supercage of FAU, which is fully consistent with the mass spectrometry results. In contrast, the Ni(II) sites were heavily blocked by the bulky C_2D_4 by the formation of a dynamic 1:1 adduct, which led to most of the adsorbed C_2D_4 molecules being stabilized through weak hydrogen bonding and intermolecular guest-guest interactions. Similar host-guest binding interactions were observed in the structure models of $[Ni_{12}Na_{20}(Al_{44}Si_{148}O_{384})]\cdot(C_3D_4)_{20}$ and $[Ni_{12}Na_{20}(Al_{44}Si_{148}O_{384})]\cdot(C_3D_6)_{26}$ with C···Ni distances of 3.96 and 4.56 Å, respectively (only one binding site observed in each model; Fig. 3, D and E). Thus, the distinct nature of sorbent-gas interaction construed the high selectivity of Ni@FAU toward alkyne adsorption.

To visualize the binding dynamics of adsorbed C_2H_2 and C_2H_4 molecules, inelastic neutron scattering (INS) studies were conducted with Ni@FAU as a function of gas loading at 5 K (figs. S43 to S48). Compared with the INS spectra of solid C_2H_2 and C_2H_4, the difference INS spectra (i.e., signals of adsorbed gas molecules) had differences in the low-energy region (<30 meV) that were correlated to the translation and libration modes of molecular vibration. In the solid state, molecules interact with adjacent ones in all three dimensions (figs. S49 to S54 and table S5), which results in coupling and dispersion of the modes (*23*). When adsorbed onto Ni(II) sites, gas molecules become isolated and restricted in an anisotropic environment, which results in distinct INS features. The peak frequencies and (anisotropic) amplitude were directly dictated by the Ni(II)-gas interactions and the local environment.

We assigned the sharp and intense INS peaks at 3.8 meV for bound C_2H_2 (peak I) and 2.5 to 3.8 meV for adsorbed C_2H_4 (peaks I′ and II′) to the motion of gas molecules within the plane perpendicular to the Ni(II)-gas axis, because these vibrational modes are the least hindered and had the lowest frequencies and largest displacement. These INS spectra were in marked agreement with the binding sites elucidated by NPD, in terms of peak I correlating to the sole binding site of C_2H_2, whereas peaks I′ and II′ resulting from the two C_2H_4 sites with the former being the major adsorption site. Peak I for bound C_2H_2 occurred at a higher average energy, which confirmed that the interaction between Ni@FAU and C_2H_2 was stronger than that of C_2H_4.

Additionally, adsorbed gas molecules may rotate or twist around the axis perpendicular to the Ni(II)-gas axis and move toward or away from the Ni(II) sites, contributing to the peaks at 10 to 15 meV and at 15 to 30 meV, respectively. Moreover, the trans- and cis-C–H bending modes for bound C_2H_2 at 81.5 and 99 meV, respectively, were blue-shifted compared with those of solid C_2H_2 (80 and 95 meV, respectively; Fig. 4A), which indicates that these internal modes were strongly hindered upon binding on the Ni(II) sites. In contrast, no apparent shift was observed for the in-plane C–H rocking mode of C_2H_4 at 102 meV upon adsorption (Fig. 4B). Overall, the INS study showed marked agreement with NPD, adsorption, and breakthrough results, and it identified the crucial role of confined Ni(II) sites on the chemoselective binding of C_2H_2 in Ni@FAU.

Solid-sorbent–based techniques hold increasing promise to improve the operational efficiency of existing separation processes in petrochemical industries, and the separation of alkyne impurities from olefins can only be realized by exploiting the differences in their properties, such as dimensions (*24*, *25*), shapes (*26*), conformation (*27*), polarisabilities (*4*), coordination abilities (*28*), binding affinity (*29*), and the geometry-matching with the sorbent pores (*30*). Zeolites with well-defined channels have been considered to be viable candidates for gas separation for decades, primarily on the basis of their molecular sieving property (*12*). By confining atomically dispersed Ni(II) sites in the FAU zeolite channels, the discrimination between alkyne and olefin binding was amplified in Ni@FAU, which enabled the production of polymer-grade olefins under conditions relevant to practical processes. Combining its facile synthesis at large scale and its notable stability, the Ni@FAU sorbent offers a potential practical solution to the challenging alkyne/olefin separations.

REFERENCES AND NOTES

1. D. S. Sholl, R. P. Lively, *Nature* **532**, 435–437 (2016).
2. H. Zimmermann, R. Walzl, in *Ullmann's Encyclopedia of Industrial Chemistry* (Wiley, 2000).
3. A. Borodziński, G. C. Bond, *Catal. Rev., Sci. Eng.* **48**, 91–144 (2006).
4. X. Cui *et al.*, *Science* **353**, 141–144 (2016).
5. S.-C. Xiang *et al.*, *Nat. Commun.* **2**, 204 (2011).
6. S. Yang *et al.*, *Nat. Chem.* **7**, 121–129 (2015).
7. T. L. Hu *et al.*, *Nat. Commun.* **6**, 7328–7335 (2015).
8. Y.-L. Peng *et al.*, *Angew. Chem. Int. Ed.* **57**, 10971–10975 (2018).
9. L. Li *et al.*, *J. Am. Chem. Soc.* **139**, 7733–7736 (2017).
10. L. Li *et al.*, *Angew. Chem. Int. Ed.* **57**, 15183–15188 (2018).
11. L. Yang *et al.*, *Adv. Mater.* **30**, 1705374 (2018).
12. R. T. Yang, *Gas Separation by Adsorption Processes* (Imperial College Press, 1997).
13. S. Patai, *The Chemistry of the Carbon-Carbon Triple Bond* (Wiley, 1978).
14. M. Choi, Z. Wu, E. Iglesia, *J. Am. Chem. Soc.* **132**, 9129–9137 (2010).
15. S.-W. Choi *et al.*, *J. Catal.* **345**, 113–123 (2017).
16. J. Erkelens, W. J. Wösten, *J. Catal.* **54**, 143–154 (1978).
17. M. P. Lapinski, J. G. Ekerdt, *J. Phys. Chem.* **94**, 4599–4610 (1990).
18. P. Wang *et al.*, *Angew. Chem. Int. Ed.* **56**, 8716–8720 (2017).
19. J. Lee *et al.*, *Angew. Chem. Int. Ed.* **57**, 7869–7873 (2018).
20. B. Li *et al.*, *Adv. Mater.* **29**, 1704210 (2017).
21. J. Li *et al.*, *J. Am. Chem. Soc.* **141**, 3807–3811 (2019).
22. J. H. Nelson, H. B. Jonassen, *Coord. Chem. Rev.* **6**, 27–63 (1971).
23. P. C. H. Mitchell, S. F. Parker, A. J. Ramirez-Cuesta, J. Tomkinson, *Vibrational Spectroscopy with Neutrons with Applications in Chemistry, Biology, Material Science and Catalysis* (World Scientific Publishing, 2005).
24. A. Cadiau, K. Adil, P. M. Bhatt, Y. Belmabkhout, M. Eddaoudi, *Science* **353**, 137–140 (2016).
25. P. J. Bereciartua *et al.*, *Science* **358**, 1068–1071 (2017).
26. Z. R. Herm *et al.*, *Science* **340**, 960–964 (2013).
27. P.-Q. Liao, N.-Y. Huang, W.-X. Zhang, J.-P. Zhang, X.-M. Chen, *Science* **356**, 1193–1196 (2017).
28. E. D. Bloch *et al.*, *Science* **335**, 1606–1610 (2012).
29. K. Lee, J. D. Howe, L.-C. Lin, B. Smit, J. B. Neaton, *Chem. Mater.* **27**, 668–678 (2015).
30. S. M. Kuznicki *et al.*, *Nature* **412**, 720–724 (2001).

ACKNOWLEDGMENTS

We thank C. Wang from China Petrochemical Corporation (SINOPEC) for helpful discussions. **Funding:** Supported by the National Natural Science Fund of China (21722303, 21421001, and 21688102), the Municipal Natural Science Fund of Tianjin (18JCJQJC47400 and 18JCZDJC37400), the 111 Project (B12015 and B18030), the U.K. Engineering and Physical Sciences Research Council (EP/P011632/1), and the University of Manchester and Newton Advanced Fellowship by the Royal Society (to W.S. and S.Yan.). Beamlines WISH and I11 were accessed through the STFC ISIS Facility and Diamond Light Source, respectively. INS experiments were conducted at the VISION beamline at ORNL's Spallation Neutron Source, which is supported by the Scientific User Facilities Division, Office of Basic Energy Sciences (BES), U.S. Department of Energy (DOE), under contract no. DE-AC05000R22725 with UT Battelle, LLC. The computing resources were made available through the VirtuES and the ICEMAN projects, funded by the Laboratory Directed Research and Development program at ORNL. **Author contributions:** Y.Cha. conducted zeolite syntheses and performance tests. S.L. and S.Yao participated in sample characterization. C.W. and L.J. performed mass spectrometry analyses. W.S. and N.G. analyzed the data and provided helpful discussions. X.H., W.L., I.d.-S., P.M., Y.Che., L.D.D., A.J.R.-C., and C.C.T. collected and analyzed synchrotron x-ray diffraction, neutron diffraction, and INS data. S.Yan. and L.L. directed and supervised the project. Y.Cha., X.H., S.Yan., and L.L. prepared the manuscript. **Competing interests:** The authors from Nankai University are inventors of a patent (CN202010177858.0) on materials reported in this work. **Data and materials availability:** Crystallographic data for the structures reported in this article have been deposited at the Cambridge Crystallographic Data Centre under deposition numbers CCDC 1939577 to 1939585. Copies of the data can be obtained free of charge from www.ccdc.cam.ac.uk/structures/. Other data needed to evaluate the conclusions in the Report are present in the paper or the supplementary materials.

SUPPLEMENTARY MATERIALS

science.sciencemag.org/content/368/6494/1002/suppl/DC1
Materials and Methods
Supplementary Text
Figs. S1 to S55
Tables S1 to S5
References (*31*–*55*)

23 July 2019; resubmitted 16 January 2020
Accepted 10 April 2020
10.1126/science.aay8447

Science

Control of zeolite pore interior for chemoselective alkyne/olefin separations

Yuchao Chai, Xue Han, Weiyao Li, Shanshan Liu, Sikai Yao, Chong Wang, Wei Shi, Ivan da-Silva, Pascal Manuel, Yongqiang Cheng, Luke D. Daemen, Anibal J. Ramirez-Cuesta, Chiu C. Tang, Ling Jiang, Sihai Yang, Naijia Guan and Landong Li

Science **368** (6494), 1002-1006.
DOI: 10.1126/science.aay8447

Zeolites that prefer alkynes

Alkenes such as ethylene and propene must be separated from alkynes before they can be converted in polymers. Drawbacks in current methods, such as hydrogenation of alkynes producing unwanted alkanes, has spurred interest in sorption separation methods. Zeolites have generally been inefficient, given the similar sizes and volatilities of the molecules. Chai *et al.* incorporated atomically dispersed divalent transition metal cations into faujasite zeolite and found that the nickel-containing analog efficiently removed alkynes from olefins through chemoselective binding at open nickel(II) sites. At ambient conditions in the presence of water and carbon dioxide, the zeolites retained separation selectivities of 100 and 92, respectively, for acetylene over ethylene and propyne over propylene for 10 adsorption-desorption cycles.

Science, this issue p. 1002